Article no. 18

THE CIVIL ENGINEERING JOURNAL 2-2020

EXPERIMENTAL STUDY ON THE SEISMIC DAMAGE OF AEOLIAN SAND CONCRETE COLUMNS WITH DIFFERENT REINFORCEMENTS

Yaohong Wang, Xiaoyan Ma, Qing Han, Qi Chu and Zeping Zhang

Inner Mongolia University of Technology, School of Civil Engineering, Hohhot, Inner Mongolia, China; wyh@imut.edu.cn, 20171800217@imut.edu.cn, 19880000016@imut.edu.cn, 20171100260@imut.edu.cn, 20171800225@imut.edu.cn

ABSTRACT

Aeolian sand is a kind of natural material with abundant reserves and a low price. Many scholars have conducted extensive studies on the engineering applications of aeolian sand. This paper addresses the seismic damage behaviour of aeolian sand concrete columns to promote the application of aeolian sand in frame structures. A total of 5 aeolian sand concrete column specimens with different reinforcements were studied using cyclic loading tests. The failure modes, stiffness degradation, bearing capacity, hysteresis peculiarity, ductility, and energy consumption of the specimens were analysed and compared. Then, applicable damage models of the specimens were proposed. The study results prove that the seismic damage behaviour of the specimens increases with the increase of longitudinal reinforcement percentage and with the transverse steel ratio when the replacement percentage of aeolian sand is constant. Additionally, the damage model which is revised in this paper agrees well with the test results. It can be used to assess the degree of damage to the aeolian sand concrete columns.

KEYWORDS

Aeolian sand, Seismic damage behaviour, Longitudinal reinforcement percentage, Transverse steel ratio

INTRODUCTION

With the worldwide development of infrastructure construction, increasing quantities of engineering sand have been exploited from rivers and mountains to meet the needs of concrete production. The mass application of ordinary engineering sand will cause vast economic costs and environmental damage. Meanwhile, the ecosystems of arid and semi-arid regions are seriously threatened by desertification where the trigger is aeolian sand. Given these circumstances, many scholars have conducted studies on concrete that uses aeolian sand to promote the harmonious coexistence of man and nature. W. Dong et al [1] studied the incorporation of aeolian sand can improve the compressive strength and tensile strength of concrete, especially for the early strength of concrete. H. F. Liu et al [2] analysed the effects of a series of mix-ratio parameters on the compressive strengths and splitting tensile strengths of aeolian-sand concrete. These mix-ratio parameters included replacement percentages of aeolian sand, coal ash content, sand ratio and water-to-binder ratio. It can be concluded that with an increase in the replacement percentage of aeolian sand and the coal ash, the strength of concrete first increased and then decreased. When the replacement percentage of aeolian sand was 20%, the strength of aeolian sand concrete reached a maximum. H. X. Yuan [3] studied the bonding properties between aeolian-sand concrete and steel bars. The results showed that the bonding properties are largely consistent with those of

ordinary reinforced concrete in 4 aspects, including concrete strength grades, anchorage lengths of steel bars, diameters of steel bars and thicknesses of protective layers. It can be demonstrated that the formula which is used to calculate adhesive property between concrete and steel bars for ordinary reinforced concrete can be applied to aeolian-sand concrete. G. Q. Wang et al [4] studied the seismic behaviour of 2 specimens which included an ordinary sand concrete column and a aeolian-sand concrete column using a cyclic loading test. The results showed that the seismic damage behaviour of aeolian sand concrete columns is superior to that of ordinary sand concrete columns. H. P. Yin et al [5] carried out a low-cycle repeated load test with an ordinary concrete column and 4 fully recycled concrete columns. The test results manifested that the bearing capacity, stiffness and energy consumption of the columns improved on increasing in the reinforcement percentage of recycled aggregate. Y. Q. Zhang et al [6] conducted experimental research on 5 short recycled concrete columns with different transverse steel ratios. The test and analysis results indicated that the ductility, bearing capacity and energy consumption of the short recycled concrete columns improved with increasing of the transverse steel ratio. However, when the transverse steel ratio exceeded a certain limit, the extent of improvement of the above behaviours was limited.

At present, domestic and foreign scholars have made quite achievements in the application of desert sand in concrete. However, most of the research work focuses on the study of the mechanical properties of desert sand concrete. Only a few scholars have conducted experimental research on the performance of desert sand concrete specimens. Based on existing results, this paper studies the seismic damage to aeolian sand concrete columns with different reinforcement configurations. Cyclic loading tests and damage analyses for 5 concrete column specimens were used to achieve the study objectives. The failure modes, stiffness degradation, bearing capacity, hysteresis peculiarity, ductility, and energy consumption of the specimens were analysed and compared. Then, an applicable damage model of the specimens was proposed.

TEST PROGRAM

Details of specimen

The specimens include 5 columns with the same geometric dimensions, shear span ratios and axial compression ratios. The specimens are designated ASC1, ASC2, ASC3, ASC4 and ASC5. The replacement percentage of aeolian sand for all specimens is 20%. The calculated height of each specimen is 875 mm, and the section dimensions of each column are 250 mm x 250 mm. The characteristics of the columns are displayed in Table 1.Details of aeolian sand concrete columns are displayed in Figure 1.

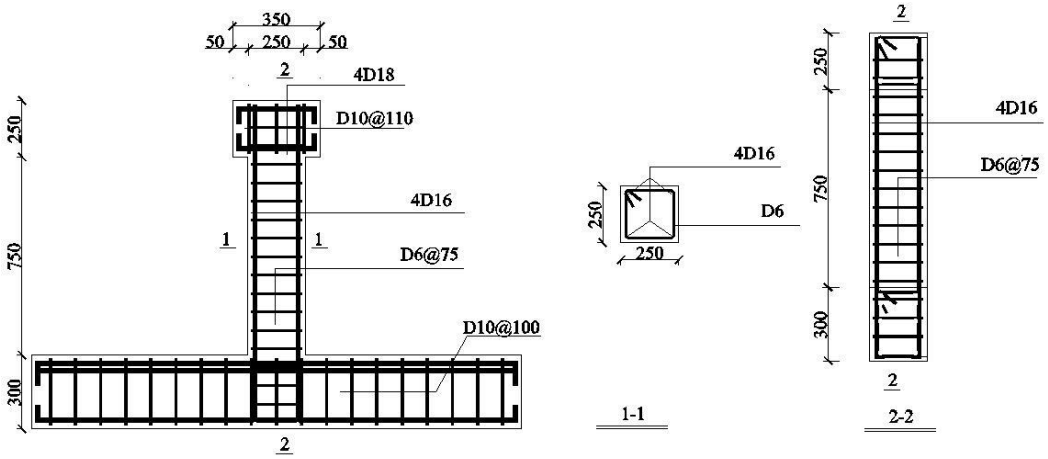

Fig. 1 – Details of aeolian sand concrete columns (a)ASC1

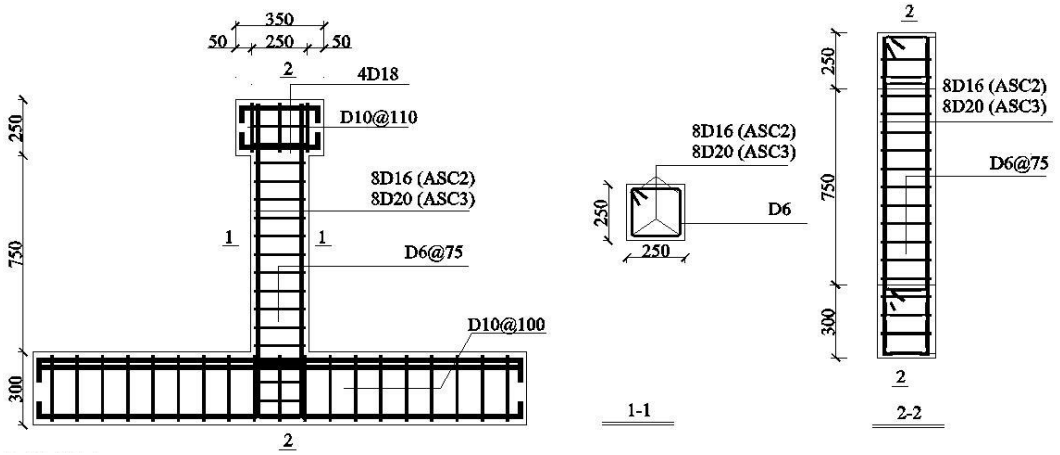

(b) ASC2, ASC3

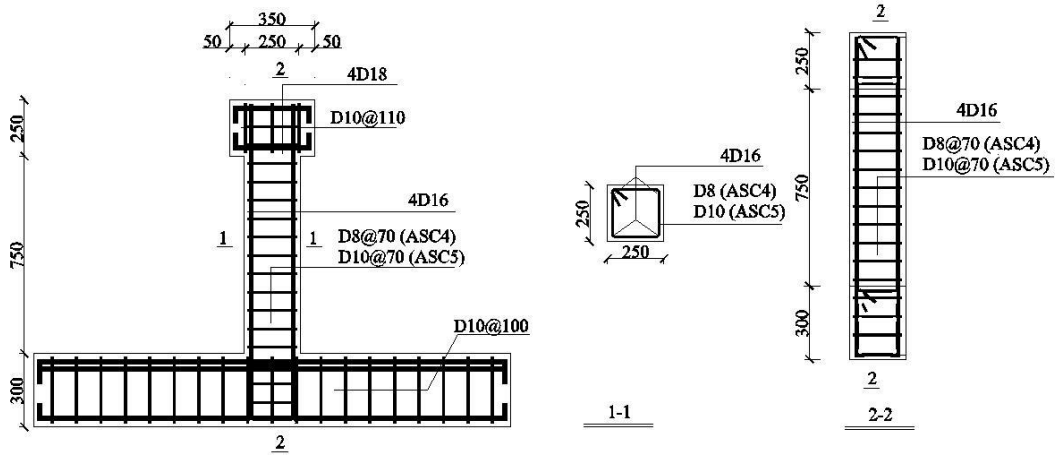

(c) ASC4, ASC5

Fig. 1 – Details of aeolian sand concrete columns

Tab. 1 - Characteristics of the columns

Specimen number	ASC1	ASC2	ASC3	ASC4	ASC5
Axial compression ratio	0.2	0.2	0.2	0.2	0.2
Shear span ratio	3.5	3.5	3.5	3.5	3.5
Longitudinal reinforcement percentage	1.20%	2.30%	3.50%	1.20%	1.20%
Transverse steel ratio	0.60%	0.60%	0.60%	1.00%	1.40%

Material properties

The concrete of 5 columns is the same group. The types of material sand mix ratio of concrete are displayed in Table 2 below. The cubic compressive strength can be measured through using a compression machine, which is displayed in Table 3. A tensile tester can measure the yield strength and ultimate strength, which is displayed in Table 4.

Tab. 2 - Types of materials and mix ratio of concrete

Types of materials	Water	Stone	Ordinary sand	Aeolian sand	Coal ash	Cement	Water reducer
Weight ($kg \cdot m^{-3}$)	205	1266.36	393.98	98.49	43.62	389.28	3.27

Tab. 3 - Mechanical properties of concrete

Specimen	$f_{cu,t}$/MPa
ASC1	38.3
ASC2	40.7
ASC3	36.2
ASC4	35.6
ASC5	37.1

Tab. 4 - Mechanical proprieties of steel materials

Types of reinforcement	Yield stress (MPa)	Ultimate stress (MPa)
Steel barD6	412.5	542.6
Steel bar D8	426.4	533.7
Steel bar D10	439.5	562.1
Steel bar D16	403.1	534.7
Steel bar D20	432.8	541.4

Test set-up

The cyclic loading tests were conducted at the Key Laboratory of Civil Engineering Structure and Mechanics at the Inner Mongolia University of Technology, China. The test devices are displayed in Figure 2. The height of the horizontal loading center away from the bottom of columns is 875 mm.

After the vertical pressure was applied to the vertical jack, the axial compression ratio was maintained constantly throughout the test. A horizontal low-cycle reciprocating load was applied by manipulating the pushing and stretching of the horizontal jack. In the tests, the load control method was used first. When the skeleton curve shows a significant inflection point, it is considered to enter the yield stage. Then, the displacement control method was used. The displacement of each step was integer multiples of the yield displacement. The loading continued until the bearing capacity of the specimens dropped to 85% of the peak load. In total, there were 3 electronic displacement gauges deployed in the test. They were used to measure the displacement of the specimens.

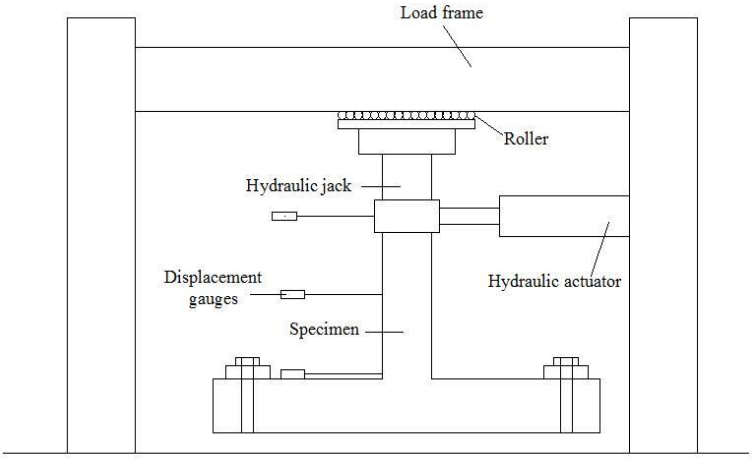

Fig. 2 –Test devices

RESULTS AND DISCUSSION

Destructive form of specimens

Specimen ASC1

As the load reached 21.8kN in the forward direction of the fourth cycle, a few horizontal cracks formed on the bottom of the column. The widths of these cracks were all approximately 1.5 mm. In the negative direction, 2 cracks formed in the middle and lower parts of the specimen. As the load reached 56.8kN, a wider crack with an angle of approximately 45° appeared approximately 300mm from the bottom of the column. The existing cracks were gradually widened. As the force reached 79.5kN, a large crack with an angle of approximately 60°formed at the bottom of the specimen, with slight spalling of the concrete. The width of this crack was approximately 5.6 mm. After this, more cracks quickly developed and intersected each other. When the specimen was broken, the concrete on the bottom of the column was crushed and peeled off over a large area. Concurrently, the stirrup and the longitudinal reinforcements were exposed and seriously buckled.

Specimen ASC2

The first cracks formed in the middle and lower parts of the column. As the positive force reached 32.8kN, a few new cracks with lengths ranging from 56 mm to 93 mm formed at the bottom of the column. When the positive force reached 83.7kN, many oblique cracks formed in the middle and lower parts of the column and were inclined downward by 30°. In the following negative direction, these oblique cracks rapidly developed and intersected each other. As the force reached 124.3kN, the existing cracks continued to expand, accompanied by the sound of cracking concrete. As the loading force was 144kN, the concrete on both sides of the bottom of the column started to peel off. As the column was destroyed, the concrete at the bottom was completely crushed. It can be observed that the stirrup and longitudinal reinforcements were exposed and yielded.

Specimen ASC3

As the force reached 68.6kN, a few new cracks with lengths ranging from 32 mm to 54 mm formed at the bottom of the column. As the force reached 138.5kN, a few new cracks with lengths ranging from 71 mm to 87 mm formed in the middle of the column. As the force increased, the cracks gradually expanded and developed. As the loading reached 153.8kN, there were a few new oblique cracks whose length was approximately 72 mm to 95 mm that formed in the middle and upper parts of the column. The development form of the existing cracks changed from length extension to width extension. The concrete in the plastic hinge area began to show signs of

loosening. When the specimen was broken, the concrete of the root segment was completely crushed and peeled off over a large area. The exposed longitudinal steel bar and stirrup were stretched and bent.

Specimen ASC4

As the load reached 43.2kN, the earliest cracks with a maximum length of 68 mm, which located in the lower part of the column. When the force was 95.8kN, there were many cracks in the middle and lower parts and almost extended obliquely down 60°. Some cracks on the right side of the root segment extended to the left with a slight peeling of the concrete. The cracks on the left side of the root segment were inclined downward 30° along the foundation beam. As the load was 147.8kN, the cracks in the middle and lower parts continued to develop. Some cracks showed a lightning shape. Subsequently, more cracks quickly developed and intersected each other. When the specimen was broken, the concrete on both sides of the root segment was crushed and peeled off. The longitudinal bar was exposed on the right side and was clearly bent. Additionally, the stirrup of the root segment was exposed and had yielded.

Specimen ASC5

As the load reached 48.4**kN** in the negative direction, the 5 earliest cracks formed in the lower parts of the column. The cracks developed rapidly and were distributed horizontally. As the load was 138.5**kN**, some cracks in the lower part showed a lightning shape and penetrated each other. On the right side, a crack of 56 mm in length extended from the root segment of the specimen to the middle and lower parts of the specimen and followed an angle of approximately 60°. As the peak load was 158.3**kN**, the largest crack in the root segment of the specimen widened to 4.2 mm. Concurrently, the concrete of the root segment began to partially peel off. When the specimen was broken, the concrete of the root segment was completely crushed and peeled off over large areas. The results indicated that the stirrup and longitudinal reinforcement were exposed and had seriously buckled.

The destructive forms of the specimens are displayed in Figure 3. The details of damage when the specimens were broken are displayed in Figure 4. During the tests, the failure processes of the specimens were recorded in detail. When the specimens were under the same load, the degree of damage decreased with an increase in the longitudinal reinforcement percentage and in the transverse steel ratio.

(a)ASC1 *(b)ASC2* *(c)ASC3* *(d)ASC4* *(e)ASC5*

Fig. 3 – The destructive form of the specimens

(a)ASC1 (b)ASC2 (c)ASC3 (d)ASC4 (e)ASC5

Fig. 4 – Details of damage when the specimens were broken

Skeleton and hysteresis curves of specimens

The hysteresis and skeleton curves for the 5 specimens are shown in Figures 5 and 6. The figures show that the specimens are basically in an elastic stage at the beginning of each test. The hysteresis curves rise along an approximately straight line during this period. With the continuous increase in force value and displacement, the hysteresis curves change flexibly. The residual strain increases continuously. Additionally, the stiffness gradually degenerates. After the specimens yielded, the horizontal displacements rise significantly faster than the horizontal loads. After the force reaches its peak load, the bearing capacity declines with the number of load augments. In general, for the specimens whose reinforcements have been strengthened, the bearing capacity decreases more slowly, and the hysteresis curves are relatively fuller. This indicates that they have stronger energy dissipation capacities.

From a comparison of the hysteresis curves and skeleton curves of specimens ASC1 to ASC3, we observe some rules, which are mentioned next. Due to the earlier cracking of concrete, specimen ASC1 shows a more obvious pinching phenomenon, which leads to a significantly lower energy consumption and poorer hysteresis performance of the specimen compared to others 4 specimens. The maximum loads of the columns gradually increase with the increase of longitudinal reinforcement percentages and transverse steel ratios. The reinforcement using longitudinal reinforcement can assist the specimens in withstanding axial pressures and in reducing creep deformation and cross-sectional dimension. Thus, this reinforcement can effectively enhance the bearing capacity of aeolian sand concrete specimens to increase the longitudinal reinforcement percentage.

From the comparison of the hysteresis and skeleton curves of specimens ASC1, ASC4 and ASC5, we can present some rules as follows. Specimens ASC4 and ASC5, with smaller stirrup spacing, show relatively gentle transitions in the skeleton curves. The bearing capacity of these 2 specimens declines more slowly than that of specimen ASC1. In other words, the maximum load per loading cycle of specimens gradually rises with the increases in the transverse steel ratio and with a decrease in stirrup spacing. This increase is because the stirrup can effectively prevent the development of oblique cracks and enhance the synergistic work between the concrete and the steel bars. Thus, this is an effective method to enhance the bearing capacity of aeolian sand concrete specimens by increasing the transverse steel ratio.

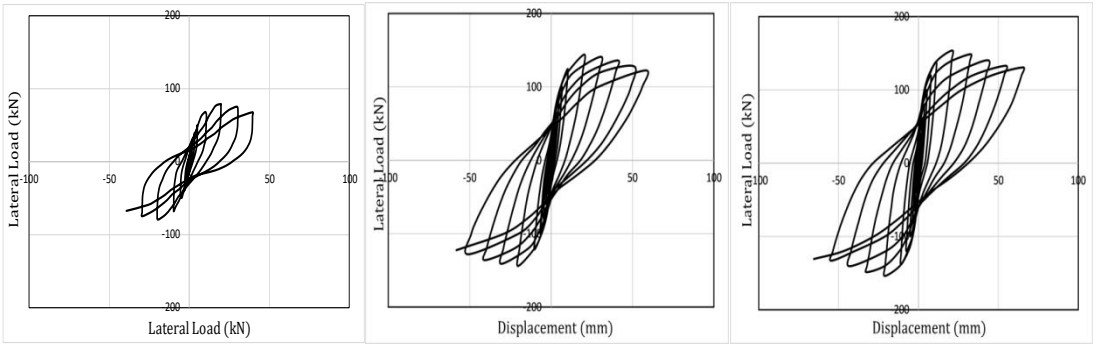

(a) ASC1 *(b) ASC2* *(c) ASC3*

(d) ASC4 *(e) ASC5*

Fig. 5 – Hysteresis curves of the columns

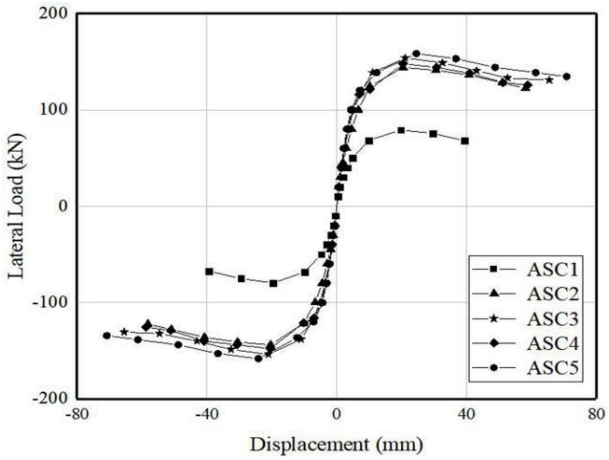

Fig. 6 – Skeleton curves of the columns

Feature points and ductility of columns

The feature points of specimens measured are shown in Table 5. In Table 5, F_{cr} is the cracking load and Δ_{cr} is the cracking displacement. F_y is the load at the time of yielding of the specimen and Δ_y is the yield displacement. F_{max} is the maximum horizontal load and Δ_{max} is the displacement. When loading is lower than 85% of the peak load, the specimen declared failed. At this point, Δ_u is the displacement displacement and F_u is the load when the specimen is failed.

Tab. 5 - Loading capacity of columns

Specimen	Original cracking		Yielding		Ultimate stage		Failure stage	
	F_{cr} (kN)	Δ_{cr} (mm)	F_y (kN)	Δ_y (mm)	F_{max} (kN)	Δ_{max} (mm)	F_u (kN)	Δ_u (mm)
ASC1	21.8	0.98	68.31	9.85	79.65	19.7	67.7	39.5
ASC2	32.8	1.84	124.3	10.19	144	20.38	122.4	58.2
ASC3	35.4	2.01	138.2	11.02	153.8	21.08	130.73	65.48
ASC4	43.2	1.96	121.2	10.23	147.8	20.46	125.6	58.83
ASC5	48.4	2.08	133.5	12.26	158.3	24.53	134.5	70.86

The displacement ductility coefficients of columns measured are shown in Table 6. The formula for calculating the ductility coefficient is Δ_u/Δ_y. There are many methods used by scholars to judge the yield of specimens. The energy equivalent method [7] was used in this paper.

Tab. 6 - Ductility coefficients of columns

Specimen	Ductility coefficient	Relative value of the ductility coefficient
ASC1	4.01	1
ASC2	5.71	1.42
ASC3	5.94	1.48
ASC4	5.75	1.43
ASC5	5.78	1.44

From Tables 5 and 6, we can draw the following conclusions:

The ductility coefficient of specimen ASC1 is the smallest of all specimens. It indicates that the aeolian sand concrete column specimens have relatively better ductility.

Compared with ASC1, specimens ASC2 and ASC3 have an increase in bearing capacity of 80.79% and 93.09%, respectively. The ductility coefficients of the 3 specimens increased approximately linearly as the increase in the longitudinal reinforcement percentage.

Compared with ASC1, specimens ASC4 and ASC5, with greater transverse steel ratios and smaller stirrup spacing, have higher ultimate deformations and bearing capacities. This is mainly because the strengthening of the edge constraint of the specimen increases the frictional bite force of the crack surfaces. This effect can resist the slip failure of oblique shear planes and delay the development of concrete cracks. This effect is conducive to allow the full expression of the plastic deformation ability of various materials.

In all, strengthening the longitudinal reinforcement percentage and the transverse steel ratio can markedly improve the ductility and bearing capacity of aeolian sand concrete specimens. We can further consider enhancing the replacement percentage of aeolian sand for economic reasons without sacrificing seismic damage behaviour of the specimens.

Energy dissipation

The amounts of energy consumption while the loading process is indicated by the area of the hysteresis loop. Thus, the accumulation of the area of every hysteresis loop area indicates the

total energy consumption of the specimen. The experiment results of the cumulative energy consumption of the specimens are displayed in Figure 7 and Table 7. By comparing of the energy consumption of specimens ASC1 to ASC5, we can specify some rules as follows. The energy consumption of specimen ASC1 is the smallest of all specimens. The maximum energy consumption can reach almost 5.0 times that of the ASC1. The energy consumption of specimen ASC3 increased by 27.2% over that of the ASC2. The energy consumption of specimen ASC5 is increased by 7.3% that over of the ASC4. We conclude that the energy consumption of the columns strongly increases as an increase in the longitudinal reinforcement percentage and with increases in the transverse steel ratio. In other words, the aeolian sand concrete column specimens with enhanced reinforcement can absorb more seismic energy. These columns show a better energy-consuming effect, and this is helpful for avoiding the collapse of aeolian-sand concrete structures in large earthquakes.

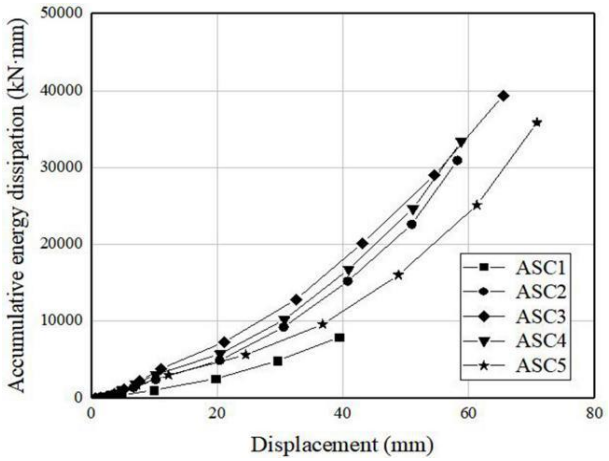

Fig. 7 –*Accumulative energy consumption of columns*

Tab. 7 - Cumulative energy consumption of the columns

Specimen	Cumulative energy consumption (kN·mm)	Cumulative energy consumption ratio
ASC1	7,918.930	1
ASC2	30,929.808	3.91
ASC3	39,357.441	4.94
ASC4	33,401.500	4.22
ASC5	35,833.941	4.53

Stiffness degradation

The stiffness degradation can fully reflect the damage process of specimens from cracking to plastic deformation. The stiffness can be calculated according to the following formula [8].

$$k_{x,i} = \frac{|+F_{x,i}|+|-F_{x,i}|}{|+X_{x,i}|+|-X_{x,i}|} \quad (1)$$

Where $+F_{x,i}$ is the maximum point in the forward direction of i-th loading cycle, $-F_{x,i}$ is the maximum point in the negative direction of i-th loading cycle, $+X_{x,i}$ is the displacement of i-th cycle

maximum point in the forward direction, and $-X_{x,i}$ is the i-th cycle maximum point displacement in the negative direction. As the horizontal displacement increases, the stiffness of each specimen is significantly reduced. After the specimens had cracked, the maximum point load value and maximum point displacement for every cycle were got through the test result. Then, the secant stiffness of each loading cycle was calculated. The calculation results are displayed in Table 8. The stiffness degradation curves of columns are displayed in Figure 8.

Tab. 8 - Stiffness of the columns

ASC1		ASC2		ASC3		ASC4		ASC5	
$k_{x,i}$	n	$k_{x,i}$	n	$k_{x,i}$	n	$k_{x,i}$	n	$k_{x,i}$	n
25.35	1	29.85	1	30.3	1	30.07	1	29.4	1
20.4	0.8	27.27	0.91	27.21	0.9	27.4	0.91	28.1	0.96
16.44	0.65	23.31	0.78	24.79	0.82	25.1	0.83	26.43	0.9
12.36	0.49	20.13	0.67	22.21	0.73	23.12	0.77	25	0.85
10.34	0.41	17.7	0.59	19.38	0.64	20.66	0.69	22.52	0.77
6.93	0.27	14.99	0.5	15.52	0.51	16.57	0.55	16.59	0.56
4.03	0.16	12.06	0.4	12.55	0.41	11.85	0.39	11.09	0.38
2.55	0.1	7.07	0.24	7.3	0.24	7.22	0.24	6.5	0.22
1.72	0.07	4.61	0.15	4.57	0.15	4.69	0.16	4.17	0.14
——	——	3.34	0.11	3.26	0.11	3.4	0.11	2.95	0.1
——	——	2.51	0.08	2.43	0.08	2.52	0.08	2.26	0.08
——	——	2.1	0.07	2	0.07	2.13	0.07	1.9	0.06

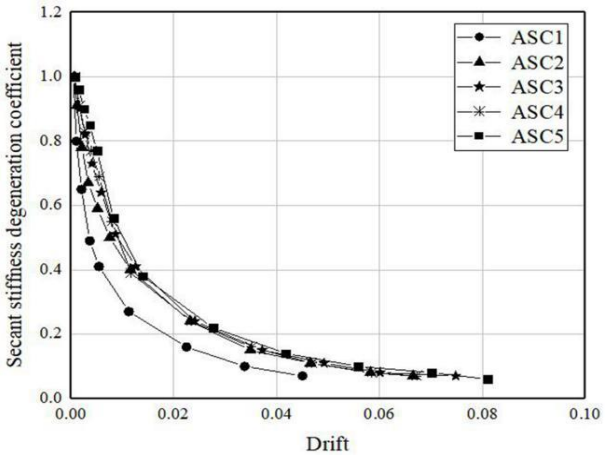

Fig. 8 –Stiffness degradation curves of columns

From the comparison of the stiffness degradation of specimens ASC1 to ASC3, we observe that the stiffness degradation speed of column ASC1 is the highest. At the initial stage of testing, concrete can contribute much to the specimen stiffness. After a specimen has cracked, the concrete in the tension zone is withdrawn from work. Then, the contribution of the longitudinal reinforcement in the tension zone to the stiffness of the specimens increases. Thus, both the initial and cracking stiffness values of the specimens are improved with an increase in the longitudinal reinforcement percentage.

From comparisons of the stiffness degradations of specimens ASC1, ASC4 and ASC5, we observed that specimens ASC4 and ASC5 have the slowest stiffness degradations during loading

the test. This is because the stirrups provide an effective lateral constraint for the specimens. The stiffness degradation of the columns is naturally improved. Therefore, that can effectively improve the stiffness degradation of the columns through increasing the transverse steel ratios.

DAMAGE MODEL

The study of the seismic damage behaviour of structures needs to involve an analysis of the damage evolution process. The damage model can measurably describe the extent of damage to structures. There are many kinds of damage assessment models, most of which have their own advantages and disadvantages. In this paper, the single-parameter damage model based on deformation and the two-parameter damage model based on deformation and energy are used to analyse the entire process of seismic damage evolution of the specimens.

Fajfar damage model-single parameter

The Fajfar model [9] uses elastic-plastic deformation to reflect the degree of damage. This model considers that the damage is caused by maximum elastoplastic deformation of the structure or of a member. The expression is:

$$D_1 = \frac{X_m - X_y}{X_u - X_y} \qquad (2)$$

In Equation (2), X_m and X_y are the maximum elastoplastic deformation and yield deformation of the structure or component under cyclic loading, respectively and X_u is the limit deformation of the structure or component under cycle loading. Although this model does not consider fatigue effects, its expression is simple and easy to apply. The Fajfar model assumes that the specimen is in an elastic phase before yielding and that its damage is negligible. As the cyclic displacement increases, the damage index, D, gradually increases in a linear manner. When the bearing capacity of specimen drops to 85% of the maximum load capacity, the limit displacement reaches X_u, and the damage index, D, of the specimen reaches a value of 1.0. The specimen is defined as broken at this time. The calculation results of the specimens, which use Equation (2), are shown in Table 9.

Niu Ditao and Ren Lijiedamage model two-parameter

The existing study results show that the damage to a structure under earthquake motion is not only related to the maximum deformation but is also related to the cumulative damage. Therefore, it is difficult to reflect the low-cycle fatigue effect on a structure if we only use the maximum displacement to evaluate structural damage. This practice has shown that it is more reasonable to use the two-parameter model to evaluate the seismic damage behaviour of specimens. Niu Ditao and Ren Lijie [10] proposed a damage assessment model. It is based upon deformation and energy consumption through actual seismic damage calculation and analysis. The expression is:

$$D_2 = \frac{X_m}{X_u} + \alpha\left(\frac{E_h}{E_u}\right)^{\beta} \qquad (3)$$

In Equation (3), X_u is the limit displacement of the specimen under cycle loading and X_m and E_h are the maximum displacement and cumulative energy consumption of the column under cyclic loading, respectively. α and β are combination coefficients, reflecting the effects of deformation and energy dissipation, respectively. Niu et al. analysed the degree of damage to an actual structure in an earthquake damage investigation, and determined that $\alpha = 0.1387$ and $\beta = 0.0814$. This model uses X_m/X_u and E_h/E_u to represent the degree of damage caused by deformation and by energy consumption, respectively. This model considers the nonlinear problem and the relationship between deformation and energy. Bringing the original values of α and β into this paper, we find that the degree of damage to specimens is larger than the actual situation in

tests. Therefore, the combination coefficient in Equation (3) was revised in this paper to be consistent with test results through statistical fitting methods. The revised expression is as follows:

$$D_2 = \frac{X_m}{X_u} + 0.067\left(\frac{E_h}{E_u}\right)^{0.65} \quad (4)$$

The calculation results of the specimens, which use Equation (4), are shown in Table 9.

Tab. 9 - Calculation results for D1 and D2

Specimen	ρ_w	ρ_s	X_m/mm	E_h/(kN·mm)	D_1	D_2
ASC1	0.6%	1.2%	19.70	2,498.98	0.33	0.53
			29.55	4,848.72	0.67	0.80
			39.40	7,918.93	1.00	1.00
ASC2	0.6%	2.3%	20.38	4,897.46	0.21	0.37
			30.57	9,235.81	0.42	0.56
			40.76	15,210.01	0.64	0.74
			50.95	22,607.41	0.85	0.93
			61.14	30,929.81	1.00	1.00
ASC3	0.6%	3.5%	21.08	7,286.12	0.18	0.35
			32.56	12,844.41	0.40	0.53
			43.08	20,172.46	0.59	0.70
			54.60	29,022.16	0.80	0.89
			66.12	39,357.44	1.00	1.01
ASC4	1.0%	1.2%	20.46	5,753.49	0.21	0.37
			30.69	10,235.09	0.42	0.55
			40.92	16,767.49	0.63	0.74
			51.15	24,641.74	0.84	0.92
			61.38	33,401.50	1.00	1.04
ASC5	1.4%	1.2%	24.53	5,615.69	0.21	0.37
			36.78	9,593.69	0.42	0.55
			48.82	16,011.89	0.63	0.74
			61.30	25,106.52	0.85	0.93
			73.56	35,833.94	1.00	1.05

In Table 9, ρ_w is the transverse steel ratio. ρ_s is the longitudinal reinforcement percentage. X_m is the maximum displacement during cyclic loading. E_h is the cumulative energy dissipation during cyclic loading. D_1 is the calculation result of equation (2). D_2 is the calculation result of equation (4).

Table 9 shows that D_1 is less than D_2. The latter value is more consistent with the test process of the specimens used. We conclude that the two-parameter damage model, as revised in the article, is consistent with the actual situation. It is feasible to use this model to analyse the entire damage process of aeolian sand concrete column specimens.

CONCLUSIONS

This paper studies the seismic damage behaviour of aeolian-sand concrete columns. A total of 5 aeolian sand concrete column specimens with different reinforcement configurations were studied on the basis of cyclic loading tests. Then, an applicable damage model of the specimens was proposed. The conclusion is as below:

(1) When under the same load, the degree of damage to aeolian sand concrete column specimens decrease with increasing of the longitudinal reinforcement percentage and transverse steel ratio.

(2) Increasing the longitudinal reinforcement percentages and transverse steel ratios can effectively improve the stiffness degradation, bearing capacity, ductility and energy consumption of aeolian sand concrete column specimens.

(3) From the test and analysis results, we conclude that increasing the replacement percentage of aeolian sand while increasing the longitudinal reinforcement percentages and transverse steel ratios, results in no sacrifice in the seismic damage behaviour of the specimens.

(4) The two-parameter damage model, which is revised in the article, can be used to analyse the entire damage process of aeolian sand concrete column specimens.

ACKNOWLEDGEMENT

This paper is subsidized by the National Natural Science Foundation of China (51868059).

REFERENCES

[1] W. Dong, et al.2018. Effect of aeolian sand and fly ash content on mechanical properties of concrete. Bulletin of Silicate, 37(7), 237-242.
[2] H. F. Liu, J. R. Ma,J. Fu,et al. 2015. Study on mechanical properties of desert sand concrete. Concrete (9), 80-83. (in Chinese).
[3] H. X. Yuan. 2018. Study on Bonding Performance between Sand Concrete and HRB400 Reinforcing Bar[D]. Xinjiang University, 2018.(Doctoral dissertation in Chinese).
[4] G. Q. Wang, Z. Q. Li , S. Yang, et al. 2018. Experimental study on seismic behavior of desert sand concrete frame columns under cyclic loading. Concrete (6).(in Chinese).
[5] H. P. Yin. 2010. Experimental study on seismic behavior of recycled concrete columns with different reinforcement ratios. Earthquake Disaster Prevention Technology, 5(1), 99-107.(in Chinese).
[6] Y. Q. Zhang. 2011. Experimental study on seismic behavior of short concrete columns with different hoop ratios. Building Structure (s1), 272-276.(in Chinese).
[7] J. G. Nie , L. Zhu, et al. 2013. Experimental study on seismic behavior of steel plate shear wall. Journal of Building Structures, 34(1), 61-69.

[8] JGJ 101-96. 1997.Specificating of Testing Methods for Earthquake Resistant Building, China Architecture & Building Press, Beijing, China.(in Chinese)
[9] Fajfar, P. . 2010. Equivalent ductility factors, taking into account low-cycle fatigue. Earthquake Engineering & Structural Dynamics, 21(10), 837-848.
[10] D. T. Niu, L. J. Ren. 1996. Improved two-parameter seismic damage model for reinforced concrete structures. Earthquake Engineering and Engineering Vibration (4), 44-54. (in Chinese).